Molecular Structure of the Oxidized, Recombinant, Heterocyst [2Fe–2S] Ferredoxin from *Anabaena* 7120 Determined to 1.7-Å Resolution[†,‡]

Bruce L. Jacobson,[§] Young Kee Chae,[∥,⊥] John L. Markley,[⊥] Ivan Rayment,[§,⊥] and Hazel M. Holden*[,§,⊥]

Institute for Enzyme Research, Graduate School, Graduate Program in Biophysics, and Department of Biochemistry, University of Wisconsin, Madison, Wisconsin 53705

Received February 19, 1993; Revised Manuscript Received April 13, 1993

ABSTRACT: The [2Fe–2S] ferredoxin produced in the heterocyst cells of *Anabaena* 7120 plays a key role in nitrogen fixation, where it serves as an electron acceptor from various sources and an electron donor to nitrogenase. The three-dimensional structure of this ferredoxin has now been determined and refined to a crystallographic *R* value of 16.7%, with all measured X-ray data from 30.0 to 1.7 Å. The molecular motif of this ferredoxin is similar to that of other plant-type ferredoxins with the iron–sulfur cluster located toward the outer edge of the molecule and the irons tetrahedrally coordinated by both inorganic sulfurs and sulfurs provided by protein cysteinyl residues. The overall secondary structure of the molecule consists of seven strands of β-pleated sheet, two α-helices, and seven type I turns. It is of special interest that 4 of the 22 amino acid positions thought to be absolutely conserved in nonhalophilic ferredoxins are different in the heterocyst form of the protein. Three of these positions are located in the metal–cluster binding loop.

Some cyanobacteria, such as *Anabaena* 7120, are capable of nitrogen fixation, whereby N_2 is reduced to NH_3. This process requires an anaerobic environment, which is achieved through specialized cells referred to as heterocysts. These heterocyst cells arise from the normal, vegetative cells of the cyanobacterium in response to low levels of reduced nitrogen. Intercellular connections, maintained between the vegetative and heterocyst cells, allow for free exchange of products from both photosynthesis and nitrogen fixation.

Two biochemically distinct [2Fe–2S] ferredoxins have been purified and characterized from the vegetative and heterocyst forms of *Anabaena* 7120 (Schrautemeier & Böhme, 1985; Böhme & Schrautemeier, 1989), and their structural genes have been isolated and sequenced (Böhme & Haselkorn, 1989; Alam *et al.*, 1986). The ferredoxin encoded by *petF* is expressed primarily in vegetative cells and in low levels in heterocyst cells (Böhme & Haselkorn, 1989). In contrast, the other, encoded by *fdxH*, is expressed only in heterocyst cells (Alam *et al.*, 1986). While the ferredoxin encoded by *petF* presumably couples photosynthetic electron transport to a variety of oxidation–reduction reactions, the heterocyst ferredoxin acts as an immediate electron donor to nitrogenase, the enzyme responsible for the reduction of N_2 to NH_3.

The vegetative and heterocyst ferredoxins isolated from *Anabaena* 7120 differ in midpoint oxidation–reduction potentials, amino acid compositions, immunological cross-reactivities, and electron spin resonance spectra (Böhme & Schrautemeier, 1989). A comparison of their amino acid sequences reveals 50 of 98 amino acid residues to be absolutely conserved, thus corresponding to a 51% identity in primary structure. In addition, the heterocyst protein differs from other plant-type [2Fe–2S] ferredoxins in 4 of the 22 positions thought to be conserved in nonhalophilic ferredoxin amino acid sequences (Matsubara & Hase, 1983).

In general, the [2Fe–2S] ferredoxins are typically low molecular weight proteins displaying oxidation–reduction potentials between −305 and −455 mV (Cammack *et al.*, 1977). The three-dimensional structures of four such plant-type proteins have been determined thus far, namely, those isolated from the cyanobacteria *Spirulina platensis*, *Aphanothece sacrum*, and *Anabaena* 7120 and that obtained from the *Halobacterium* of the Dead Sea (Fukuyama *et al.*, 1980; Tsukihara *et al.*, 1981, 1990; Rypniewski *et al.*, 1990; Sussman *et al.*, 1989). In addition, the domain that binds the [2Fe–2S] metal center in phthalate dioxygenase reductase has been shown recently to have a similar molecular fold (Correll *et al.*, 1992). Unlike the plant-type ferredoxins, however, the midpoint oxidation–reduction potential for this [2Fe–2S] cluster is −174 mV (Correll *et al.*, 1992). All of the above-mentioned proteins display similar molecular motifs, with four major strands of β-pleated sheet and two α-helices. The metal clusters are located toward the outer edges of these molecules and are ligated to the proteins via cysteinyl residues.

Herein we describe the X-ray crystallographic structure determination to 1.7-Å resolution of the heterocyst form of the [2Fe–2S] ferredoxin isolated from *Anabaena* 7120, and we compare its molecular architecture to that previously determined for the vegetative ferredoxin (Rypniewski *et al.*, 1990).

EXPERIMENTAL PROCEDURES

Crystallization and X-ray Data Collection. Oxidized, recombinant heterocyst [2Fe–2S] ferredoxin was prepared as described elsewhere (Jacobson *et al.*, 1992). Crystals were grown by vapor diffusion from 2.2 M ammonium sulfate, 50 mM sodium succinate, and 5 mM sodium azide (pH 4.5) at room temperature and under atmospheric oxygen, as previously described (Jacobson *et al.*, 1992). The crystals belonged to the space group $P6_5$ with unit cell dimensions of $a = b = 44.2$ Å and $c = 80.6$ Å, and they contained one molecule per asymmetric unit.

[†] This research was supported in part by grants from the NIH (GM30982 to H.M.H. and GM35976 to J.L.M.) and Grant 1104 from the New Energy and Industrial Development Organization of Japan (to J.L.M.). H.M.H. is an Established Investigator of the American Heart Association.

[‡] X-ray coordinates for heterocyst ferredoxin have been deposited in the Brookhaven Protein Data Bank and may be accessed under filename 1FRD or directly from the authors at HOLDEN@ENZYME.MACC.EDU(Internet) or HOLDEN@WISCMACC(BITNET).

* Author to whom correspondence should be addressed.
[§] Institute for Enzyme Research, Graduate School.
[∥] Graduate Program in Biophysics.
[⊥] Department of Biochemistry.

0006-2960/93/0432-6788$04.00/0

Table I: Intensity Statistics

	resolution range (Å)											
	∞ to 5.80	4.10	3.35	2.90	2.60	2.37	2.20	2.05	1.94	1.84	1.75	1.68
average intensity	1378	1740	1292	693	452	306	241	200	132	92	66	54
average σ	63.8	77.4	63.1	44.2	34.1	29.6	26.9	22.5	18.1	17.0	16.4	16.2
R factor[a]	0.026	0.027	0.032	0.044	0.055	0.071	0.084	0.084	0.102	0.139	0.189	0.220

[a] R factor = $\Sigma|I - \bar{I}|/\Sigma I$.

X-ray data were collected at 4 °C with a Siemens X1000D area detector system. The X-ray source was nickel-filtered copper Kα radiation from a Rigaku RU200 X-ray generator operated at 50 kV and 50 mA. An X-ray data set to 1.7-Å resolution was collected from a single crystal with overall dimensions of 0.6 × 0.6 × 0.6 mm. These X-ray data were processed with the data reduction software package XDS (Kabsch, 1988) and internally scaled according to the algorithm of Fox and Holmes (1966) as implemented by Dr. Phil Evans. Friedel pairs were measured for all reflections, and the X-ray data set was 99% complete to 1.7-Å resolution. Relevant X-ray data collection statistics may be found in Table I.

Structure Determination. The large, anomalous signal arising from the metal cluster made it possible to locate the positions of the two iron atoms in the asymmetric unit by a difference Patterson map calculated with coefficients of the form $|F_{hkl}-F_{\bar{h}\bar{k}\bar{l}}|^2$. At this point in the investigation, it was not known whether the space group was $P6_1$ or $P6_5$. In each of these enantiomorphic space groups, however, there are Harker peaks located at $w = {}^1/_6, {}^1/_3, {}^1/_2, {}^2/_3$, and ${}^5/_6$. Shown in Figure 1 are three of these Harker sections from an anomalous difference Patterson map calculated with all X-ray data from 30.0- to 1.7-Å resolution and contoured at 2σ. From the anomalous difference Patterson map, the two irons in the metal center were located at the following positions, as expressed in hexagonal fractional coordinates: Fe site I $x = 0.327$, $y = 0.593$, $z = 0.000$; Fe site II $x = 0.365$, $y = 0.573$, $z = 0.018$. It is important to note that the following is an equally valid solution: Fe site I $x = 0.327$, $y = 0.593$, $z = 0.000$; Fe site II $x = 0.365$, $y = 0.573$, $z = -0.018$.

The heterocyst form of the ferredoxin is 51% homologous to the protein derived from vegetative cells and contains the same number of amino acid residues. It was thus possible to solve the structure of the heterocyst ferredoxin by an R factor search employing the refined X-ray coordinates of the vegetative ferredoxin as the search model (B. L. Jacobson, H. Cheng, J. L. Markley, & H. M. Holden, manuscript in preparation). In each space group, there are two valid solutions for the positions of the iron atoms as given above. Also, it was not known whether Fe site I, determined from the Patterson map, corresponded to Fe site I in the search model or rather to Fe site II. Consequently, for each space group, there were four possible orientations by which the irons of the known model could be superimposed onto the positions of the irons of the unknown structure. For all eight orientations, the known model was placed into the unit cell according to the iron positions as determined from the Patterson maps and then systematically rotated about the line defined by these irons. R factors were calculated with all X-ray data from 30.0 to 5.0 Å at intervals of 5°. Results from the R factor searches in both space groups are shown in Figure 2. The R factors were typically 55–60% except when the model, in space group $P6_5$, was rotated by 265° from the starting position, with Fe I of the model corresponding to $x = 0.365$, $y = 0.573$, $z = 0.018$ and Fe II of the model corresponding to $x = 0.327$, $y = 0.593$, $z = 0.000$. At that position, the R factor was 39.9%. The lowest R factor calculated in the space group $P6_1$ was 49.2%.

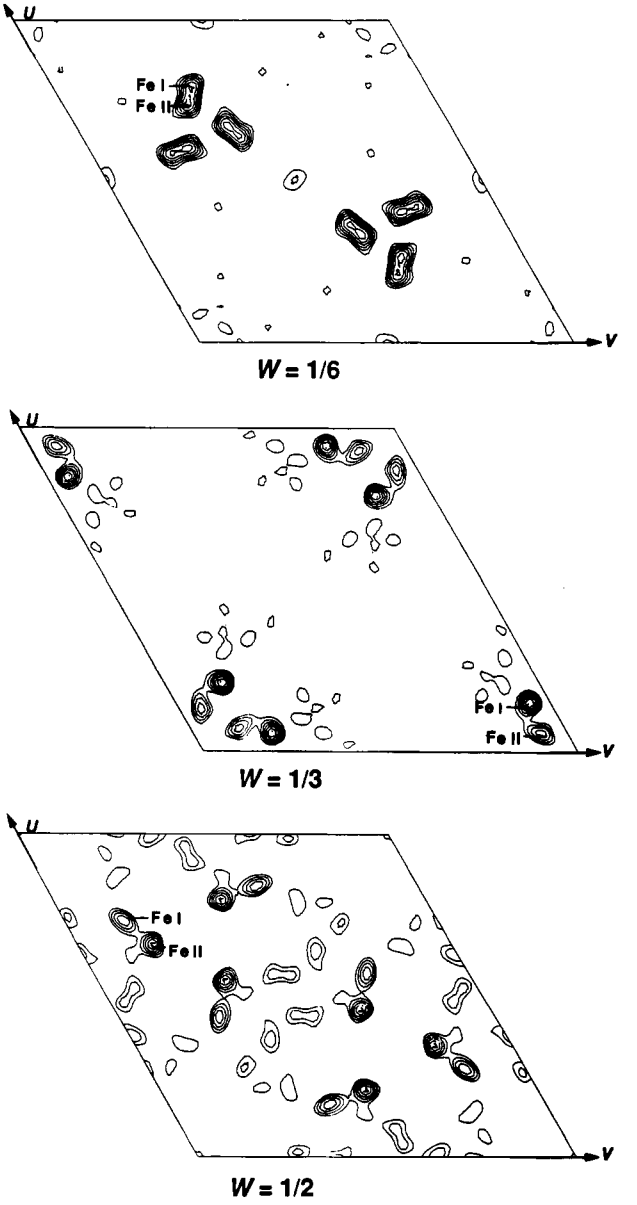

FIGURE 1: Harker sections for the native anomalous difference Patterson map. (a, top) The section of the native anomalous difference Patterson map shown here was calculated with coefficients of the form $|F_{hkl}-F_{\bar{h}\bar{k}\bar{l}}|^2$ and corresponds to $w = {}^1/_6$. The map was contoured at 2σ and increasing in increments of 1σ. An entire unit cell in the u and v direction has been plotted. The positions of the iron atoms in the cluster were originally solved in the space group $P6_1$. Harker peaks arising from these sites at $u = x - y$ and $v = x$ are indicated by the arrows. (b, middle) The iron sites indicated by the arrows correspond to the Harker peaks at $u = 2x - y$, $v = x + y$, and $w = {}^1/_3$. (c, bottom) Shown here are the positions of the Harker peaks arising at $u = 2x$, $v = 2y$, and $w = {}^1/_2$.

Once the orientation of the heterocyst ferredoxin in the unit cell was known, the model was subjected to alternating cycles of least-squares refinement with the software package

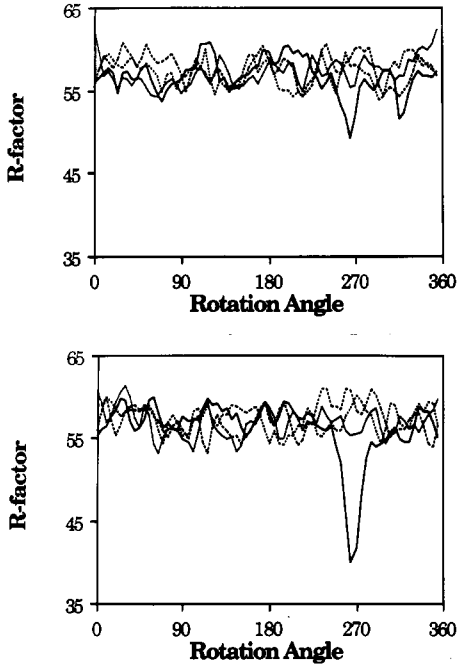

FIGURE 2: Plot of R factor *versus* rotation angle. (a, top) As described in the text, there were four possible modes in which the positions of the two irons in the search model could be superimposed onto the positions of the irons in an unknown structure. Results from R factor searches of these four modes conducted in the space group $P6_1$ are shown here. The minimum R factor (49.2%) occurred at a rotation angle of 270°. (b, bottom) Results from the four R factor searches conducted in the space group $P6_5$ are shown. As can be seen, the minimum R factor (39.9%) occurred at a rotation angle of 265°.

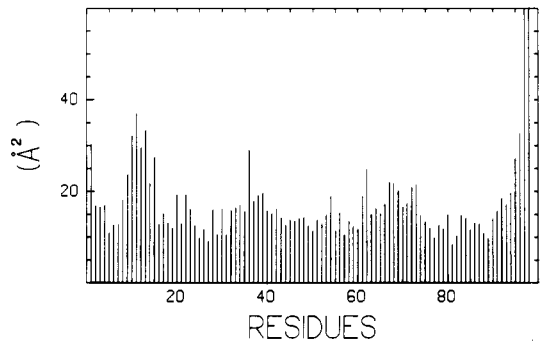

FIGURE 3: Plot of the mean B value *versus* amino acid residue for all main-chain atoms. Most of the temperature factors for the backbone atoms were well below 30 Å², except those for the last two C-terminal residues. Excluding amino acid residues Leu 97 and Ala 98, the average B value was 15.8 Å² for backbone atoms.

TNT (Tronrud *et al.*, 1987) and manual model building. A total of 58 solvent molecules were positioned into the electron density map, with 23 having temperature factors below 30 Å². The average temperature factors for the solvent and the [2Fe–2S] cluster were 37.2 and 13.1 Å², respectively. During the early stages of the refinement, "ideal" stereochemistry for the [2Fe–2S] cluster was based on the small-molecule structure determination of $(Et_4N)_2[FeS(SCH_2)_2C_6H_4]_2$ by Mayerle *et al.* (1973). Toward the end of the refinement and model building, the iron–sulfur cluster geometry was not restrained. A plot of the mean main-chain temperature factors *versus* amino acid residue numbers may be found in Figure 3. Results from the least-squares refinement may be found in Table II.

RESULTS

The molecular structure of the oxidized, recombinant, heterocyst [2Fe–2S] ferredoxin from *Anabaena* 7120 has been determined and refined to a crystallographic R factor of 16.7%, with all X-ray data from 30 to 1.7 Å. A representative portion of the electron density map is given in Figure 4. The electron density was very well-ordered except for several surface residues (Lys 10, Glu 23, Glu 31, Glu 36, Lys 52, Glu 69, Lys 73, and Tyr 96), the last two residues at the C-terminus, and C^δ of Ile 64. A plot of the main-chain dihedral angles is given in Figure 5.

Those amino acid residues participating in the formation of secondary structural elements are listed in Table III. As in other plant-type [2Fe–2S] ferredoxins, the molecular architecture of the heterocyst protein is predominantly characterized by five β-strands forming a mixed sheet motif, as depicted in Figures 6 and 7. These β-strands are labeled A–E in Table III. Note, however, that β-strand D, delineated

Table II: Refinement Statistics

resolution limits (Å)	30.0–1.7
R factor (%)[a]	16.7
no. of reflections used	9743
no. of protein atoms	759
no. of solvent molecules	58
weighted root-mean-square deviations from ideality	
bond length (Å)	0.009
bond angle (deg)	2.931
planarity (trigonal) (Å)	0.007
planarity (other planes) (Å)	0.007
torsion angle (deg)[b]	16.896

[a] R factor = $\Sigma|F_o - F_c|/\Sigma|F_o|$. [b] The torsion angles were not restrained during the refinement.

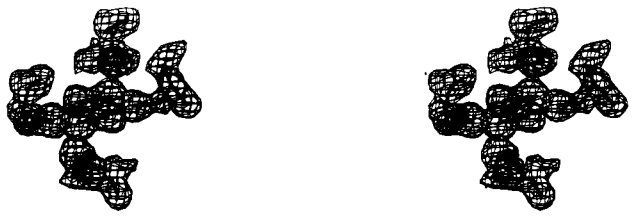

FIGURE 4: Representative portion of the electron density map. The electron density shown corresponds to the [2Fe–2S] cluster and the cysteinyl ligands. The electron density map was calculated with coefficients of the form $[2F_o-F_c]$ and contoured at 1σ.

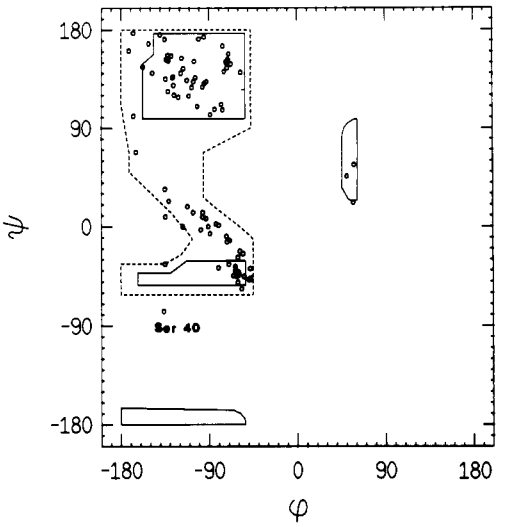

FIGURE 5: Ramachandran plot of all non-glycinyl main-chain dihedral angles for the ferredoxin model. Fully allowed ϕ,ψ values are enclosed by solid lines; those only partially allowed are enclosed by dashed lines. The only amino acid residue that lies outside of the allowed regions is Ser 40, which is located near the cluster and in the vicinity of a symmetry-related molecule in the crystalline lattice. The electron density in this region is very well-ordered.

Table III: List of Secondary Structural Elements

amino acid residues	structure type
1–9 (A)	β-pleated sheet
10–13	type I turn
14–21 (B)	β-pleated sheet
21–24	type I turn
26–31	α-helix
47–50	type I turn
51–53 (C)	β-pleated sheet
57–59 (C)	β-pleated sheet
60–63	type I turn
68–72	α-helix
71–74	type I turn
75–77 (D)	β-pleated sheet
77–80	type I turn
81–83 (E)	β-pleated sheet
87–91 (E)	β-pleated sheet
94–97	type I turn

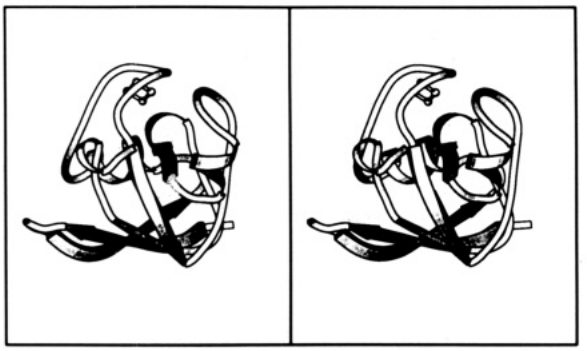

FIGURE 6: Ribbon representation of the heterocyst ferredoxin. This figure was prepared with the software MOLSCRIPT (Kraulis, 1991). The protein is characterized by four major strands of β-sheet, one short strand of β-sheet, two α-helices, and seven type I reverse turns. The metal center, displayed as a ball-and-stick model, is located at the outer edge of the protein in a loop region.

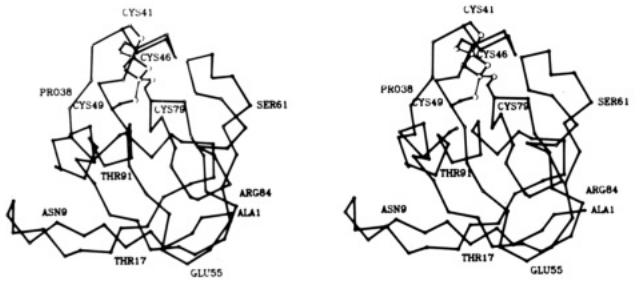

FIGURE 7: Stereoview of an α-carbon trace of the heterocyst ferredoxin. The orientation of the model shown here is the same as in Figure 6. The iron–sulfur cluster, depicted as an atomic model, is ligated to the protein via the cysteinyl sulfurs of residues 41, 46, 49, and 79.

by Phe 75 to Leu 77, is rather short with only three residues. Also, β-strands C and E are interrupted such that technically there are seven strands of β-sheet rather than five. In addition to these strands of β-sheet, the molecule contains two α-helices and seven type I reverse turns. The ϕ,ψ angles for these turns are given in Table IV.

Of the 58 solvent molecules that have been identified from the electron density map, 7 are observed in identical locations in the vegetative ferredoxin (Jacobson *et al.*, manuscript in preparation). Temperature factors for these conserved solvent molecules range from 16.0 to 25.4 Å^2. Two of these putative water molecules are located at the surface of the protein and serve to link the backbone amide hydrogens of Thr 25 and Asp 58 to the carboxylate groups of Asp 28 and Glu 57, respectively. Another solvent molecule bridges the carbonyl oxygen of Val 80 to the amide hydrogen of Asp 62. Both Val

Table IV: List of Reverse Turns

amino acid residues	type	ϕ_2	ψ_2	ϕ_3	ψ_3
10–13	I	−47.9	−38.2	−90.6	−0.1
21–24	I	−68.7	−12.7	−96.5	8.7
47–50	I	−47.6	−47.1	−96.3	12.7
60–63	I	−58.4	−22.5	−82.8	2.3
71–74	I	−62.9	−34.6	−80.2	1.0
77–80	I	−55.2	−24.8	−71.5	−14.0
94–97	I	−60.4	−28.1	−88.9	−6.5

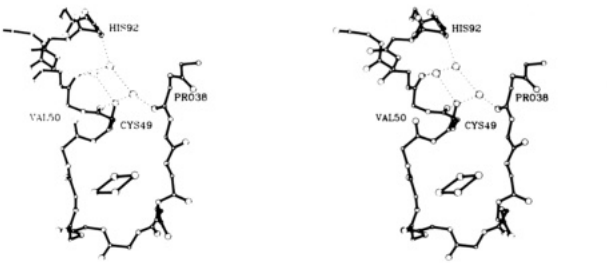

FIGURE 8: Structurally conserved solvent molecules. In both the heterocyst and vegetative forms of the ferredoxin, three solvent molecules form a channel leading from the interior to the exterior of the protein, as shown here in stereo. The [2Fe–2S] cluster is located toward the lower half of the figure. For the sake of simplicity only main-chain atoms are displayed. Potential hydrogen-bonding interactions for these solvent molecules are represented as dashed lines and range in length from 2.7 to 3.0 Å. The most buried of these water molecules is within hydrogen-bonding distance of the carbonyl oxygens of Pro 38 and Cys 49 and another solvent molecule. The second water molecule resides within hydrogen-bonding distance of the backbone amide nitrogen of His 92 and the carbonyl oxygen of Val 50. Finally, the third water, located closer to the surface, is within hydrogen-bonding distance of the carbonyl oxygens of Ser 48 and Val 50.

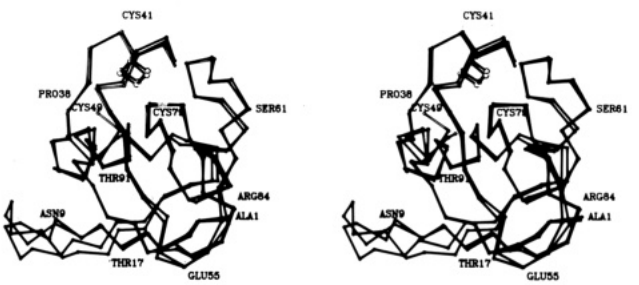

FIGURE 9: Superposition of the heterocyst and vegetative ferredoxins isolated from *Anabaena* 7120. The heterocyst form of the protein is shown in solid bonds, while the vegetative form is shown in open bonds. The two proteins were superimposed according to the algorithm of Rossmann and Argos (1972). X-ray coordinates for the vegetative ferredoxin were determined and refined to 1.7-Å resolution (Jacobson *et al.*, manuscript in preparation).

80 and Asp 62 are located in type I turns. The fourth conserved water molecule caps the end of the α-helix defined by amino acid residues Asp 68 to Gly 72 by hydrogen bonding to the carbonyl oxygens of Met 71 and Phe 75 and the side-chain nitrogen of Gln 60. Three of these structurally conserved solvent molecules form a channel leading from the interior of the protein to the surface, as shown in Figure 8. The most buried of these three water molecules is 6.7 Å from Fe II of the iron–sulfur center and is within hydrogen-bonding distance of the carbonyl oxygens of Pro 38 and Cys 49. As can be seen in Figure 8, this solvent molecule may play a role in stabilizing the cluster binding loop by bridging these regions of the polypeptide chain together.

A superposition of the vegetative and heterocyst ferredoxin models is shown in Figure 9. The α-carbon positions for these two proteins superimpose with a root-mean-square value of 1.0 Å. As can be seen, the only significant differences in the

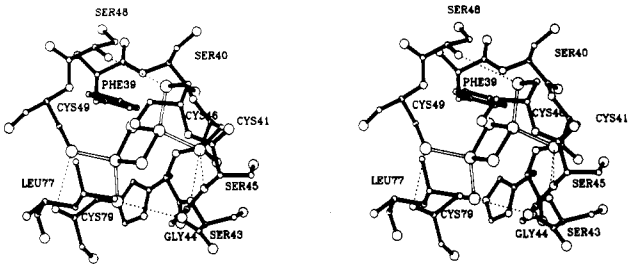

FIGURE 10: Close-up view of the iron–sulfur cluster binding site. Those amino acid residues that are within 4.0 Å of atoms in the [2Fe–2S] cluster are displayed. Potential hydrogen bonds from the protein to the inorganic sulfur atoms in the cluster and to the cysteine sulfurs are indicated by dashed lines.

Table V: Potential Hydrogen Bonds around the [2Fe–2S] Cluster

atoms involved in H-bonds	distance[a] (Å) vegetative	heterocyst
S^{γ} of Cys 41 and N of Ser 43	3.1	3.2
S^{γ} of Cys 41 and N of Ser 45	3.4	3.4
S^{γ} of Cys 46 and N of Ser 48	3.4	3.4
S^{γ} of Cys 49 and N of Cys 79	3.4	3.6
S^{γ} of Cys 79 and N of Gly 44	3.6	3.6

[a] Distances were based on X-ray coordinates refined at 1.7-Å resolution (Jacobson *et al.*, manuscript in preparation).

polypeptide chain backbone between these ferredoxins occur in the loop delineated by Ile 9 and Thr 24 and the three C-terminal residues. Excluding these regions, the α-carbons for these molecules superimpose with a root-mean-square value of 0.45 Å. The different conformations of amino acid residues Asn 9 to Thr 24 in the vegetative and heterocyst proteins are due to both crystal packing interactions and amino acid sequence differences. In the vegetative ferredoxin, Glu 10 is involved in a hydrogen bond to Lys 93. In the heterocyst model, residue 10 is a lysine, and residue 93 is a glutamine. Although these are potentially compensatory changes, residue 90 is also a lysine, and N^{ζ} of its side chain is in a position to disrupt the interactions between Lys 10 and Glu 93. Consequently, in the heterocyst protein, Lys 10 instead forms a strong hydrogen bond to $O^{\gamma 2}$ of Asp 59 in a symmetry-related molecule, stabilizing a different backbone conformation. The net result is that the type I turn which occurs between Asn 9 and Glu 12 in the vegetative model is shifted to Lys 10 and Ile 13 in the heterocyst ferredoxin.

A close-up view of the metal cluster binding pocket is shown in Figure 10. Potential hydrogen-bonding interactions between backbone amide hydrogens and sulfurs of the cysteinyl ligands and inorganic sulfurs of the cluster are indicated by the dashed lines. The hydrogen-bonding pattern around the [2Fe–2S] cluster in the heterocyst ferredoxin is nearly identical to that observed in the vegetative form of the protein. A list of the hydrogen-bonding distances may be found in Table V.

The vegetative and heterocyst ferredoxins each contain 98 amino acid residues, 50 of which are absolutely conserved between the two proteins. In the heterocyst ferredoxin, 4 of the 22 amino acid positions thought to be conserved in nonhalophilic ferredoxins are not retained (Matsubara & Hase, 1983). Three of these residues, His 42, Ser 43, and Leu 78, are located near the iron–sulfur cluster. In other nonhalophilic ferredoxins these residues are typically arginine, alanine, and threonine, respectively. The other nonconserved residue in the heterocyst ferredoxin is Ala 76, which is typically a valine residue.

The histidine at position 42 is of special interest in that it is strictly conserved in 22 of the 24 nonhalophilic plant-type

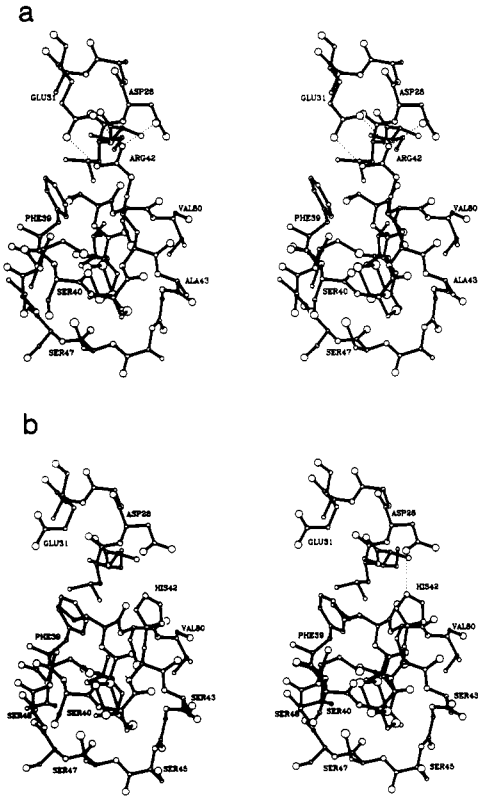

FIGURE 11: Comparison of the vegetative and heterocyst ferredoxin structures in the vicinity of amino acid residue 42. (a) In the vegetative ferredoxin, position 42 is an arginine residue which participates in three hydrogen bonds to Glu 31 and Asp 28, as indicated by the dashed lines. (b) In the heterocyst ferredoxin, residue 42 is a histidine. As shown by the dashed lines, His 42 participates in only one hydrogen bond to Asp 28. Note that Glu 31 adopts a different conformation in the heterocyst molecule as compared to the vegetative ferredoxin. Also, Leu 27 is more exposed to the solvent in the heterocyst protein. X-ray coordinates for the vegetative ferredoxin were determined and refined to 1.7-Å resolution (Jacobson *et al.*, manuscript in preparation).

[2Fe–2S] ferredoxins reviewed by Matsubara and Hase (1983). Moreover, Tsukihara *et al.* (1981) recognized the potential importance of this residue in folding and function. It was anticipated that the change from an arginine residue in the vegetative ferredoxin to a histidine residue in the heterocyst protein would result in local rearrangements of the polypeptide chain. As can be seen in Figure 11a,b, the two polypeptide chain backbones are, in fact, similar in this region. In the vegetative ferredoxin, however, the guanidino group of Arg 42 is anchored down by three hydrogen bonds to the carboxylates of Glu 31 and Asp 28, as indicated by the dashed lines in Figure 11a. These hydrogen bonds are between 2.7 and 2.8 Å in length. In the heterocyst molecule, His 42 participates in only one hydrogen-bonding interaction, namely, that between $N^{\delta 1}$ of the imidazole ring and the carboxylate oxygen of Asp 28, as shown in Figure 11b. The length of this putative hydrogen bond is 3.3 Å. Note that Glu 31 in the heterocyst ferredoxin swings out of the pocket, thereby altering the surface properties of the protein near the vicinity of the [2Fe–2S] cluster. The change from an arginine to a histidine residue with its fewer electrostatic interactions may serve a dual role of altering both the flexibility of the polypeptide chain and the surface properties of the protein in this region, such as the apparent increased solvent exposure of Leu 27.

One of the striking characteristics of the heterocyst ferredoxin is the "crown" of serine residues surrounding one side of the iron–sulfur cluster, as can be seen in Figure 11b.

Of the eight serine residues found in the protein, five are located in the metal binding loop at positions 40, 43, 45, 47, and 48. The binding pocket is decidedly amphipathic, with one side containing these hydrophilic residues and the other side lined with hydrophobic residues such as Leu 27, Phe 39, Val 50, Ile 64, Phe 65, Leu 77, Val 78, and Val 80. Fe I is located in the hydrophilic portion of the binding pocket, whereas Fe II is situated in the more hydrophobic region.

In summary, while most plant-type [2Fe–2S] ferredoxins exhibit both significant amino acid sequence and structural homology (Matsubara *et al.*, 1980; Fukuyama *et al.*, 1980; Tsukihara *et al.*, 1981, 1990; Rypniewski *et al.*, 1990), the structure of the heterocyst protein demonstrates that several of the supposedly invariant amino acid residues are not retained. The actual role of specific amino acid residues in controlling redox potentials, electron-transfer rates, and the interactions of the *Anabaena* ferredoxins with their redox partners is presently being investigated by site-directed mutagenesis, NMR spectroscopy, and X-ray crystallography.

REFERENCES

Alam, J., Whitaker, R. R., Krogmann, D. W., & Curtis, S. E. (1986) *J. Bacteriol. 168*, 1265–1271.

Böhme, H., & Schrautemeier, B. (1987) *Biochim. Biophys. Acta 891*, 1–7.

Böhme, H., & Haselkorn, R. (1989) *Mol. Gen. Genet. 214*, 278–285.

Cammack, R., Rao, K. K., Bargeron, C. P., Hutson, K. G., Andrew, P. W., & Rogers, L. J. (1977) *Biochem. J. 168*, 205–209.

Correll, C. C., Batie, C. J., Ballou, D. P., & Ludwig, M. L. (1992) *Science 258*, 1604–1610.

Devereux, J., Haeberli, P., & Smithies, O. (1984) *Nucleic Acids Res. 12*, 387–395.

Fox, G. C., & Holmes, K. C. (1966) *Acta Crystallogr. 20*, 886–891.

Fukuyama, K., Hase, T., Matsumoto, S., Tsukihara, T., Katsube, Y., Tanaka, N., Kakudo, M., Wada, I., & Matsubara, H. (1980) *Nature 286*, 522–523.

Jacobson, B. L., Chae, Y. K., Böhme, H., Markley, J. L., & Holden, H. M. (1992) *Arch. Biochem. Biophys. 294*, 279–281.

Kabsch, W. (1988) *J. Appl. Crystallogr. 21*, 67–71.

Kraulis, P. J. (1991) *J. Appl. Crystallogr. 24*, 946–950.

Matsubara, H., & Hase, T. (1983) *Proteins and Nucleic Acids in Plant Systematics* (Jensen, U., & Fairbrothers, D. E., Eds.) pp 168–181, Springer-Verlag, Berlin.

Matsubara, H., Hase, T., Wakabayashi, S., & Wada, K. (1980) *The Evolution of Protein Structure and Function* (Sigman, D. S., & Brazier, M. A., Eds.) pp 245–266, Academic Press, Inc., New York.

Mayerle, J. J., Frankel, R. B., Holm, R. H., Ibers, J. A., Phillips, W. D., & Weiher, J. F. (1973) *Proc. Nat. Acad. Sci. U.S.A. 70*, 2429–2433.

Rossmann, M. G., & Argos, P. (1975) *J. Biol. Chem. 250*, 7525–7532.

Rypniewski, W. R., Breiter, D. R., Benning, M. M., Wesenberg, G., Oh, B.-H., Markley, J. L., Rayment, I., & Holden, H. M. (1991) *Biochemistry 30*, 4126–4131.

Schrautemeier, B., & Böhme, H. (1985) *FEBS Lett. 184*, 304–398.

Sussman, J. L., Shoham, M., & Harel, M. (1989) *Prog. Clin. Biol. Res. 289*, 171–187.

Tronrud, D. E., Ten Eyck, L. F., & Matthews, B. W. (1987) *Acta Crystallogr., Sect. A 43*, 489–501.

Tsukihara, T., Fukuyama, K., Nakamura, M., Katsube, Y., Tanaka, N., Kakudo, M., Wada, K., Hase, T., & Matsubara, H. (1981) *J. Biochem. 90*, 1763–1773.

Tsukihara, T., Fukuyama, K., Mizushima, M., Harioka, T., Kusunoki, M., Katsube, Y., Hase, T., & Matsubara, H. (1990) *J. Mol. Biol. 216*, 399–410.